

Constrained caloric curves and phase transition for hot nuclei INDRA Collaboration

B. Borderie^a, S. Piantelli^b, M. F. Rivet^a, Ad. R. Raduta^c, G. Ademard^a,
E. Bonnet^d, R. Bougault^e, A. Chbihi^d, J.D. Frankland^d, E. Galichet^{a,f},
D. Gruyer^d, D. Guinet^g, P. Laitesse^g, N. Le Neindre^e, O. Lopez^e,
P. Marini^d, M. Pârlog^{e,c}, P. Pawlowski^h, E. Rosatoⁱ, R. Roy^j, M. Vigilanteⁱ

^a*Institut de Physique Nucléaire, CNRS-IN2P3, Université Paris-Sud 11, F-91406 Orsay
Cedex, France*

^b*INFN Sezione di Firenze, 50019 Sesto Fiorentino (FI), Italy*

^c*National Institute for Physics and Nuclear Engineering, RO-76900 Bucharest-Magurele,
Romania*

^d*GANIL, (DSM-CEA/CNRS-IN2P3), F-14076 Caen Cedex, France*

^e*LPC Caen, ENSICAEN, Université de Caen, CNRS-IN2P3 F-14050 Caen Cedex,
France*

^f*Conservatoire National des Arts et Métiers, F-75141, Paris Cedex 03, France*

^g*Université Claude Bernard Lyon 1, Institut de Physique Nucléaire, CNRS-IN2P3,
F-69622 Villeurbanne Cedex, France*

^h*Institute of Nuclear Physics, IFJ-PAN, 31-342 Kraków, Poland*

ⁱ*Dipartimento di Scienze Fisiche e Sezione INFN, Università di Napoli “Federico II”,
I-80126 Napoli, Italy*

^j*Université Laval, Québec, G1V 0A6, Canada*

Abstract

Simulations based on experimental data obtained from multifragmenting quasi-fused nuclei produced in central $^{129}\text{Xe} + ^{\text{nat}}\text{Sn}$ collisions have been used to deduce event by event freeze-out properties in the thermal excitation energy range 4-12 AMeV [Nucl. Phys. A809 (2008) 111]. From these properties and the temperatures deduced from proton transverse momentum fluctuations, constrained caloric curves have been built. At constant average volumes caloric curves exhibit a monotonic behaviour whereas for constrained pressures a backbending is observed. Such results support the existence of a first order phase transition for hot nuclei.

Keywords: Quasi-fusion reactions, nuclear multifragmentation, Caloric

One of the most important challenges of heavy-ion collisions at intermediate energies is the identification and characterization of the nuclear liquid-gas phase transition for hot nuclei, which has been theoretically predicted for nuclear matter [1, 2, 3, 4]. During the last fifteen years a big effort to accumulate experimental indications of the phase transition has been made. Statistical mechanics for finite systems appeared as a key issue to progress, revealing new first-order phase transition signatures related to thermodynamic anomalies like negative microcanonical heat capacity and bimodality of an order parameter [5, 6, 7, 8, 9]. Before this, correlated temperature and excitation energy measurements, commonly termed caloric curves, were among the first possible signatures to be studied [10, 11, 12, 13]. However in spite of the observation of a plateau in some caloric curves, no decisive conclusion related to a phase transition could be extracted [14, 15, 16]. The reason is that it is not possible to perform experiments at constant pressure or constant average volume, which is required for an unambiguous phase transition signature. Indeed, theoretical studies show that whereas many different caloric curves can be generated depending on the path followed in the thermodynamical landscape, constrained caloric curves must exhibit two behaviours if a first order phase transition is present: a monotonic evolution at constant average volume and a backbending of curves at constant pressure [17, 18].

In Ref. [19, 20] we presented simulations able to correctly reproduce most of the experimental observables measured for hot nuclei formed in central collisions (quasi-fused systems, QF, from $^{129}\text{Xe}+^{nat}\text{Sn}$, 32-50 AMeV). The aim of the present Letter is to use the event by event properties at freeze-out which were inferred from these simulations to build constrained caloric curves.

Experimental data were collected with the 4π multidetector INDRA which is described in detail in Ref. [21, 22]. Accurate particle and fragment identifications were achieved and the energy of the detected products was measured with an accuracy of 4%. Further details can be found in Ref.[23, 24, 25]. All the available experimental information (charged particle energy spectra, average and standard deviation of fragment velocity spectra and calorimetry) of selected QF sources produced in central $^{129}\text{Xe}+^{nat}\text{Sn}$ collisions which undergo multifragmentation was used.

The method for reconstructing freeze-out properties from simulations [19, 20] requires data with a very high degree of completeness, crucial for a good estimate of Coulomb energy. QF sources are reconstructed, event by event, from all the fragments and twice the charged particles emitted in the range $60 - 120^\circ$ in the reaction centre of mass, in order to exclude the major part of pre-equilibrium emission [26, 27]; with such a prescription only particles with isotropic angular distributions and constant average kinetic energies are considered. In simulations, excited fragments and particles at freeze-out are described by spheres at normal density. Then the excited fragments subsequently deexcite while flying apart. Four free parameters are adjusted to fit the data at each incident energy: the percentage of measured particles which were evaporated from primary fragments, the collective radial energy, a minimum distance between the surfaces of products at freeze-out and a limiting temperature for fragments. All the details of simulations can be found in Ref. [19, 20]. The limiting temperature, related to the vanishing of level density for fragments [28], was mandatory to reproduce the observed widths of fragment velocity spectra. Indeed, the sum of Coulomb repulsion, collective energy, thermal kinetic energy and spreading due to fragment decays accounts only for about 60-70% of those widths. By introducing a limiting temperature for fragments, the thermal kinetic energy increases, due to energy conservation, which produces the missing percentage for the widths of final velocity distributions. The agreement between experimental and simulated velocity/energy spectra for fragments, for the different beam energies, is quite remarkable (see figure 3 of [20]). Relative velocities between fragment pairs were also compared through reduced relative velocity correlation functions [29, 30] (see figure 4 of [20]). Again a good agreement is obtained between experimental data and simulations, which indicates that the retained method (freeze-out topology built up at random) and the deduced parameters are sufficiently relevant to correctly describe the freeze-out configurations, including volumes. However it should be noted that the agreement between experimental and simulated energy spectra for protons and alpha-particles (see figure 5 of [20]) is not so good; this may come from the fact that we have chosen a single value, at each incident energy, for the percentage of all measured particles which were evaporated from primary fragments to limit the number of parameters of the simulation. We shall come back to this point later.

From the simulations we deduce, event by event, various quantities needed to build constrained caloric curves, namely the thermal excitation energy of

QF hot nuclei, E^* (total excitation minus collective energy) with an estimated systematic error of around 1 AMeV, the freeze-out volume V (see envelopes of figure 8 from [20]) and the total thermal kinetic energy at freeze-out K . Events are sorted into E^* bins of 0.5 AMeV with their associated kinetic temperature T_{kin} at freeze-out. In simulations, Maxwell-Boltzmann statistics are used for particle velocity distributions at freeze-out and consequently the deduced temperatures, T_{kin} , are classical. It is important to stress here that, at present time, there is no unique thermometer and, depending on the excitation energy range, disagreements can be observed between kinetic, chemical temperatures and temperatures deduced from excited states [15, 16, 31, 32].

With regard to the pressure at freeze-out, it can be derived within the microcanonical ensemble. Let us consider fragments interacting only by Coulomb and excluded volume, which corresponds to the freeze-out configuration. Within a microcanonical ensemble, the statistical weight of a configuration C , defined by the mass, charge and internal excitation energy of each of the constituting M_C fragments, can be written as

$$W_C(A, Z, E, V) = \frac{1}{M_C!} \chi V^{M_C} \prod_{n=1}^{M_C} \left(\frac{\rho_n(\epsilon_n)}{h^3} (mA_n)^{3/2} \right) \\ \times \frac{2\pi}{\Gamma(3/2(M_C - 2))} \frac{1}{\sqrt{(\det I)}} \frac{(2\pi K)^{3/2 M_C - 4}}{(mA)^{3/2}}, \quad (1)$$

where A , Z , E and V are respectively the mass number, the atomic number, the excitation energy and the freeze-out volume of the system. E is used up in fragment formation, fragment internal excitation, fragment-fragment Coulomb interaction and thermal kinetic energy K . I is the inertial tensor of the system whereas χV^{M_C} stands for the free volume or, equivalently, accounts for inter-fragment interaction in the hard-core idealization.

The microcanonical equations of state are

$$T = \left(\frac{\partial S}{\partial E} \right)^{-1} \Big|_{V,A}, \\ P/T = \left(\frac{\partial S}{\partial V} \right) \Big|_{E,A}, \\ -\mu/T = \left(\frac{\partial S}{\partial A} \right) \Big|_{E,V}. \quad (2)$$

Taking into account that $S = \ln Z = \ln \sum_C W_C$ and that $\partial W_C / \partial V = (M_C/V) W_C$, it comes out that

$$\begin{aligned} P/T &= \left(\frac{\partial S}{\partial V} \right) = \frac{1}{\sum_C W_C} \sum_C \frac{\partial W_C}{\partial V} \\ &= \frac{1}{V} \frac{\sum_C M_C W_C}{\sum_C W_C} = \frac{\langle M_C \rangle}{V}. \end{aligned} \quad (3)$$

The microcanonical temperature is also easily deduced from its statistical definition [33]:

$$\begin{aligned} T &= \left(\frac{\partial S}{\partial E} \right)^{-1} = \left(\frac{1}{\sum_C W_C} \sum_C W_C (3/2 M_C - 5/2) / K \right)^{-1} \\ &= \langle (3/2 M_C - 5/2) / K \rangle^{-1}. \end{aligned} \quad (4)$$

As M_C , the total multiplicity at freeze-out, is large, we have

$$T \approx \frac{2}{3} \langle \frac{K}{M_C} \rangle \quad (5)$$

and the pressure P can be approximated by

$$P = T \frac{\langle M_C \rangle}{V} \approx \frac{2}{3} \frac{\langle K \rangle}{V}. \quad (6)$$

Knowing $\langle K \rangle$ and V from simulations, pressure P can be calculated for events sorted in each E^* bin. The temperature T_{kin} that we obtain from the simulations is identical to the microcanonical temperature of equation (5). One can also note that the free Fermi gas pressure exactly satisfies equation (6).

Constrained caloric curves, built with correlated values of E^* and T_{kin} have been derived for QF hot nuclei with Z restricted to the range 80-100, which corresponds to the A domain 194-238, in order to reduce effects of mass variation on caloric curves [13]; they are presented in Fig. 1. Curves for internal fragment temperatures, T_f , are also shown in the figure. For two different average freeze-out volumes corresponding to the ranges $3.0-4.0V_0$ and $5.0-6.0V_0$ - where V_0 is the volume of the QF nuclei at normal density - a monotonic behaviour of caloric curves is observed as theoretically expected. The caloric curves when pressure ranges have been selected exhibit a back-bending and moreover their qualitative evolution with increasing pressure

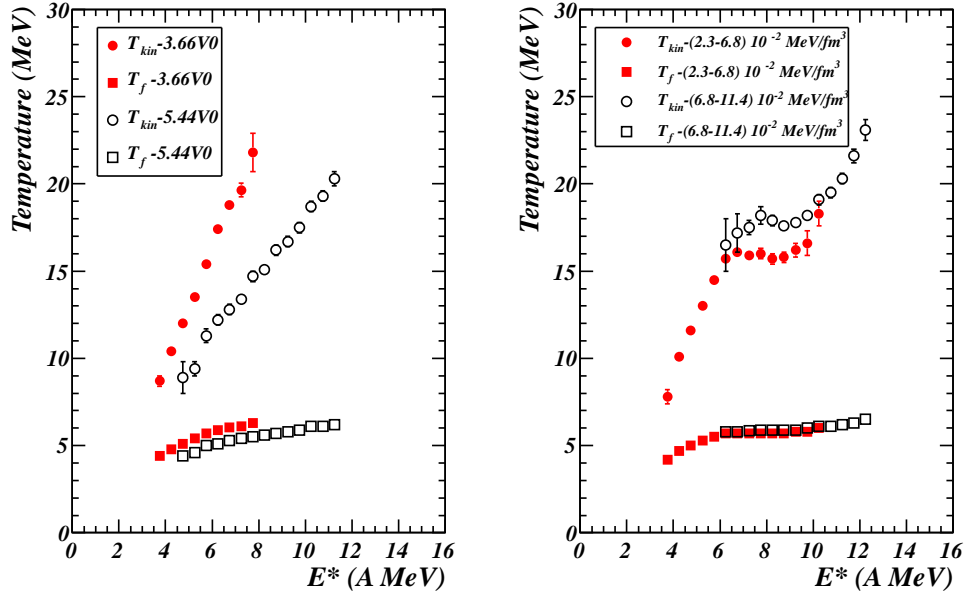


Figure 1: (Color online) Caloric curves (kinetic temperature T_{kin} versus thermal excitation energy E^*) constrained at average volumes (left) and for selected ranges of pressure (right) and the corresponding internal temperatures of fragments T_f . Error bars correspond to statistical errors.

exactly corresponds to what is theoretically predicted with a microcanonical lattice gas model [17]. The decrease of T_{kin} occurs in the E^* region where $\langle M_C \rangle / V$ increases faster with E^* than in the surrounding regions, in agreement with expected spinodal fluctuations [5].

By extrapolating to higher pressures, one could infer a critical temperature -vanishing of backbending - around 20 MeV. Such a value is within the range calculated for infinite nuclear matter whereas a lower value is expected for finite systems in relation with surface and Coulomb effects (see [16] and references therein). We thus wonder if the classical temperature T_{kin} is relevant.

Very recently a new method for measuring the temperature of hot nuclei was proposed [34, 35]. It is based on momentum fluctuations of emitted particles, like protons, in the centre of mass frame of the fragmenting nuclei. On the classical side, assuming a Maxwell-Boltzmann distribution of the momentum yields, the temperature T is deduced from the quadrupole momentum fluctuations defined in a direction transverse to the beam axis:

$$\sigma^2 = \langle Q_{xy}^2 \rangle - \langle Q_{xy} \rangle^2 = 4m^2T^2$$

with $Q_{xy} = p_x^2 - p_y^2$; m and p are the mass and linear momentum of emitted particles. Taking into account the quantum nature of particles, a correction F_{QC} related to a Fermi-Dirac distribution was also proposed [35, 36].

In that case $\sigma^2 = 4m^2T^2 F_{QC}$ where $F_{QC} = 0.2(T/\epsilon_f)^{-1.71} + 1$; $\epsilon_f = 36 (\rho/\rho_0)^{2/3}$ is the Fermi energy of nuclear matter at density ρ and ρ_0 corresponds to normal density.

Before using this new thermometer (with protons) to build constrained caloric curves, it was important to have made several verifications. With the classical simulation (freeze-out and asymptotic proton momenta), it is possible to test the agreement with the proposed classical thermometer. Moreover the effects of secondary decays on temperature measurements can be estimated. Fig. 2 shows different caloric curves without constraints. Note that the selection in Z and A of hot nuclei is the same as in the previous figure; it was also verified that, within statistical errors, at a given thermal excitation energy, transverse momentum fluctuation values are the same for our selection or by selecting only a single (A and Z) hot nucleus. Open diamonds refer to classical temperatures calculated from momentum fluctuations for protons thermally emitted at freeze-out. Within statistical errors they perfectly superimpose on unconstrained T_{kin} values. Full squares correspond to classical temperatures calculated from momentum fluctuations for protons after the secondary decay stage. We note that the caloric curve is distorted, which means that it is hazardous to use experimental data from protons to measure temperatures. Moreover, in this case, quantum corrections for temperatures can not be made because protons are emitted at different stages of deexcitation with different Fermi energy values. In Fig. 2 classical temperatures calculated from experimental proton data are also shown (full points). As for temperatures calculated from asymptotic proton data of simulations, a monotonic behaviour of the caloric curve is observed. One also notes the differences between the two sets of temperature values, which are related to the fact that, as indicated previously, simulations do not describe accurately the experimental proton energy spectra. For each E^* value the difference $\Delta T = T_{simul} - T_{exp}$ between final temperature from proton data from simulations and temperature from experimental protons will be used to correct classical temperatures derived from simulated protons at freeze-out.

It finally appears that the only way to extract temperatures from proton transverse momentum fluctuations taking into account quantum effects is to use protons thermally emitted at freeze-out. In that case classical tem-

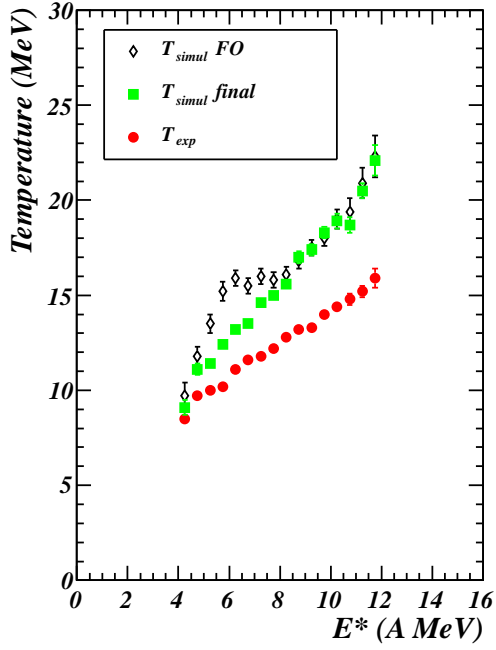


Figure 2: (Color online) Caloric curves (classical temperature from proton transverse momentum fluctuations versus thermal excitation energy) for protons (simulation) thermally emitted at freeze-out (open diamonds), for protons (simulation) after the secondary decay stage (full squares), and from protons experimentally measured (full points). Error bars correspond to statistical errors

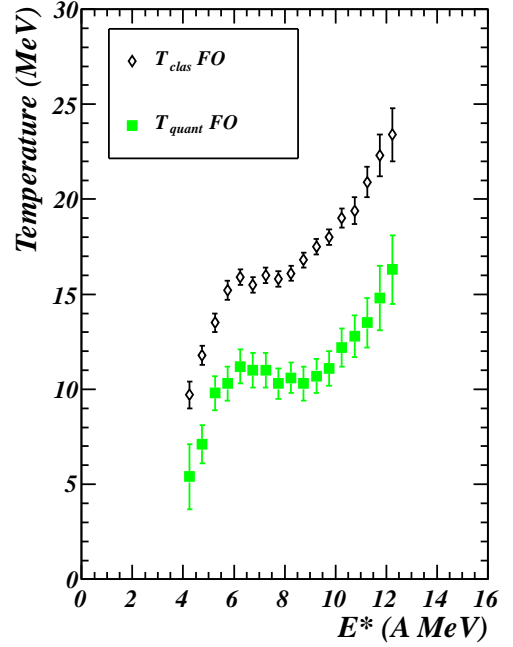


Figure 3: (Color online) Caloric curves: classical temperature (open diamonds)/ quantum corrected temperature (full squares) from proton transverse momentum fluctuations versus thermal excitation energy. Protons (simulation) are thermally emitted at freeze-out. Error bars include statistical and systematic errors.

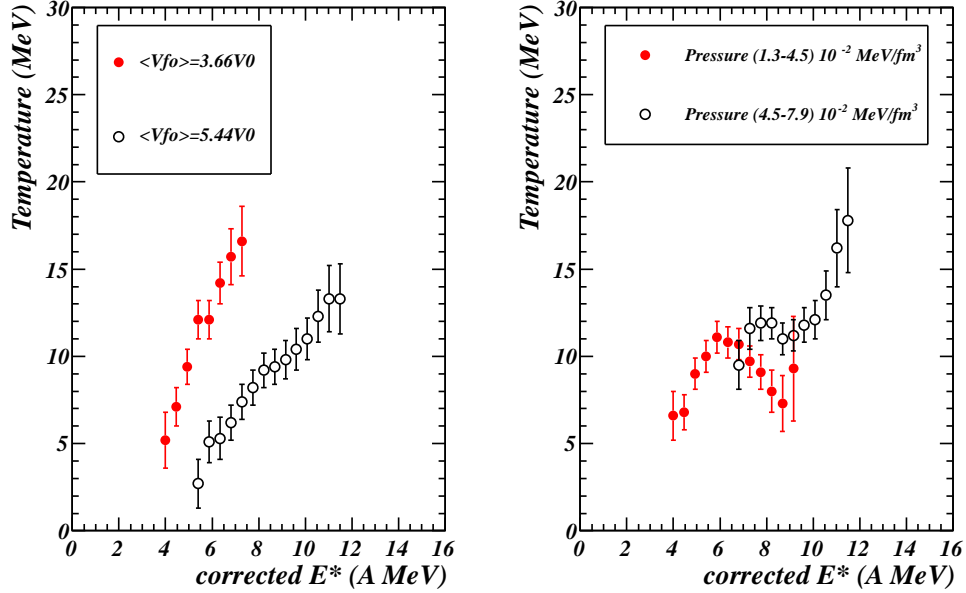


Figure 4: (Color online) Caloric curves (quantum corrected temperature versus corrected thermal excitation energy) constrained at average volumes (left) and for selected ranges of pressure (right). Error bars include statistical and systematic errors.

perature values from simulations must be extracted and corrected and then, quantum corrections applied, which needs Fermi energy values. Those values can be estimated from semi-classical calculations (Xe+Sn at 32 A MeV and Sn+Sn at 50 A MeV) [26, 37]: protons thermally emitted at freeze-out at time around 100-120 fm/c after the beginning of collisions come from a low density uniform source. For the two incident energies low densities around $\rho \sim 0.4\rho_0$ are calculated, which corresponds to $\epsilon_f \sim 20$ MeV. We have introduced a systematic error of $\pm 0.1\rho_0$ for the calculation of ϵ_f and consequently a systematic error for “quantum” temperatures of ± 0.6 to ± 0.5 MeV on the considered temperature range. Fig. 3 shows the final caloric curve with temperatures from quantum fluctuations (full squares). It exhibits a plateau around a temperature of 10-11 MeV on the E^* range 5-10 A MeV. For comparison the caloric curve with classical temperatures derived from the simulation and presented in Fig. 2 is added (open diamonds).

Constrained caloric curves, which correspond to correlated values of E^* and quantum corrected temperatures have been determined. The E^* values

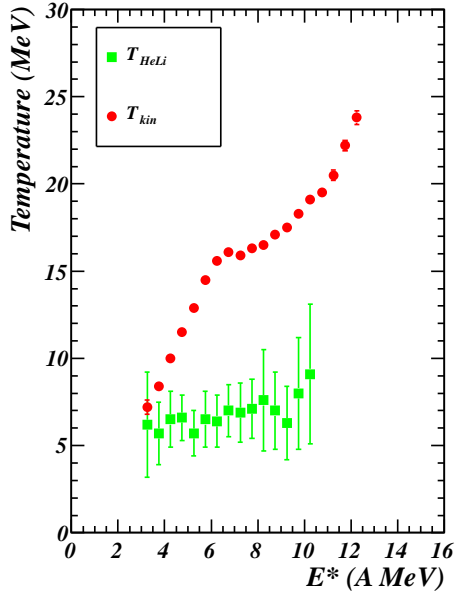


Figure 5: (Color online) Caloric curves obtained with two different temperature measurements: T_{kin} and T_{HeLi} . T_{kin} values are obtained from the simulation whereas T_{HeLi} values are derived from experimental data. Error bars correspond to statistical errors.

have been corrected *a posteriori*. Indeed they are derived from experimental calorimetry plus estimated kinetic energy for neutrons emitted at freeze-out ($E_n^{fo} = M_n^{fo} \times 3T/2$ - see [19]), which has been modified using quantum temperatures instead of classical ones. Pressure values were also corrected using quantum temperatures in equation (6). In Fig. 4 (left) we have constructed caloric curves for the two average freeze-out volumes previously chosen. Again as theoretically expected a monotonic behaviour of caloric curves is observed. Fig. 4 (right) shows the caloric curves when pressure has been constrained within two domains: $(1.3-4.5)$ and $(4.5-7.9) \times 10^{-2} \text{ MeV fm}^{-3}$. Backbending is seen especially for the lower pressure range. For higher pressures the backbending of the caloric curve is reduced and one can estimate its vanishing, indicating the critical temperature, around 13 MeV for the selected finite systems. Moreover, we can also estimate the upper limits of the spinodal region and of the coexistence region (see Fig. 2.1 of [5]) around respectively 8 and 10 A MeV. Those estimates are in good agreement (within error bars) with spinodal [38] and bimodality [9] signals.

As far as internal temperature of fragments are concerned (see Fig. 1),

one observes that the values from the simulation, T_f , perfectly agree, for our range of mass 194-238, with those calculated with the well known “He/Li thermometer” [11, 13]. We also apply this thermometer, keeping the prefactor 16 proposed in Ref. [11], to the experimental data. The derived temperature values are presented in Fig. 5 with the T_{kin} values from the simulations. We observe that the measured T_{HeLi} also exhibit a plateau and are close to the fragment temperatures, T_f , of Fig. 1. Note that, in the excitation energy range 4-10 AMeV, temperatures extracted from 5Li excited states also agree with T_{HeLi} [16, 32]. This is an indication that the temperatures obtained with the He/Li thermometer seem to reflect the internal temperature of fragments in this excitation energy range. In Ref. [13] the evolution with the mass of hot nuclei of those plateau temperatures is assimilated to that of limiting temperatures resulting from Coulomb instabilities of heated nuclei predicted long ago [39]. The following explanation can be given. For thermally equilibrated QF hot nuclei one expects internal temperature for simultaneously emitted fragments equal to the temperature of the fragmenting system, which can not exceed its Coulomb-related limiting temperature. As a direct consequence the internal fragment temperatures must reflect the evolution of this limiting temperature with the mass of hot nuclei. Such an explanation is supported by two experimental results: on one side, the fact that, on average, thermal equilibrium is achieved at the freeze-out stage [40] and, on the other side, the observation of a limitation of excitation energy for fragments on the considered E^* range [41].

In conclusion, several caloric curves have been derived for quasi-fused systems using a new thermometer based on proton transverse momentum fluctuations including quantum effects. The unconstrained caloric curve exhibits a plateau at a temperature around 10-11 MeV on the thermal excitation energy range 5-10 AMeV. For constrained caloric curves (volume or pressure) we observe what is expected for a first order phase transition for finite systems in the microcanonical ensemble, namely a monotonic behaviour at constant average volume and backbending for constrained pressure. After the observation of negative microcanonical heat capacity and bimodality of the heaviest fragment distribution, this behaviour of caloric curves is the ultimate signature of a first order phase transition for hot nuclei.

The only piece now missing is the nature of the dynamics of the transition, i.e. the fragment formation. Two mechanisms have been proposed. On one side, stochastic mean field approaches for which the fragmentation process follows the spinodal fragmentation scenario and, on the other side, molecular

dynamics (QMD, AMD) for which many-body correlations play a stronger role and pre-fragment appear at earlier times [5, 42, 43, 37, 44]. From the experimental side, signals in favor of spinodal fragmentation were observed but confidence levels around 3-4 σ prevent any definitive conclusion [45, 38]. Analyses of new experiments with higher statistics, are in progress.

References

- [1] H. Schulz et al., Phys. Lett. B 119 (1982) 12.
- [2] M. W. Curtin et al., Phys. Lett. B 123 (1983) 219.
- [3] H. R. Jaqaman et al., Phys. Rev. C 27 (1983) 2782.
- [4] H. Müller, B. D Serot, Phys. Rev. C 52 (1995) 2072.
- [5] P. Chomaz et al., Phys. Rep. 389 (2004) 263.
- [6] P. Chomaz et al. (eds.) vol. 30 of *Eur. Phys. J. A*, Springer, 2006.
- [7] B. Borderie, M.F. Rivet, Prog. Part. Nucl. Phys. 61 (2008) 551.
- [8] M. D'Agostino et al., Phys. Lett. B 473 (2000) 219.
- [9] E. Bonnet et al. (INDRA Collaboration), Phys. Rev. Lett. 103 (2009) 072701.
- [10] J. Bondorf et al., Nucl. Phys. A 444 (1985) 460.
- [11] J. Pochodzalla et al. (ALADIN Collaboration), Phys. Rev. Lett. 75 (1995) 1040.
- [12] Y. G. Ma et al. (INDRA Collaboration), Phys. Lett. B 390 (1997) 41.
- [13] J. B. Natowitz et al., Phys. Rev. C 65 (2002) 034618.
- [14] D. Durand, Nucl. Phys. A 630 (1997) 52c.
- [15] S. Das Gupta et al. in: J. W. Negele, E. Vogt (Eds), *Advances in Nuclear Physics*, vol. 26, Springer-Verlag, Berlin, 2001 p. 89.
- [16] B. Borderie, J. Phys. G: Nucl. Part. Phys. 28 (2002) R217.

- [17] P. Chomaz et al., Phys. Rev. Lett. 85 (2000) 3587.
- [18] T. Furuta, A. Ono, Phys. Rev. C 74 (2006) 014612.
- [19] S. Piantelli et al. (INDRA Collaboration), Phys. Lett. B 627 (2005) 18.
- [20] S. Piantelli et al. (INDRA Collaboration), Nucl. Phys. A 809 (2008) 111.
- [21] J. Pouthas et al., Nucl. Instr. and Meth. in Phys. Res. A 357 (1995) 418.
- [22] J. Pouthas et al., Nucl. Instr. and Meth. in Phys. Res. A 369 (1996) 222.
- [23] G. Tăbăcaru et al. (INDRA Collaboration), Nucl. Instr. and Meth. in Phys. Res. A 428 (1999) 379.
- [24] M. Pârlog et al. (INDRA Collaboration), Nucl. Instr. and Meth. in Phys. Res. A 482 (2002) 674.
- [25] M. Pârlog et al. (INDRA Collaboration), Nucl. Instr. and Meth. in Phys. Res. A 482 (2002) 693.
- [26] J. D. Frankland et al. (INDRA Collaboration), Nucl. Phys. A 689 (2001) 940.
- [27] E. Bonnet et al. (INDRA Collaboration), Nucl. Phys. A 816 (2009) 1.
- [28] S. E. Koonin, J. Randrup, Nucl. Phys. A 474 (1987) 173.
- [29] Y. D. Kim et al., Phys. Rev. C 45 (1992) 338.
- [30] G. Tăbăcaru et al. (INDRA Collaboration), Nucl. Phys. A 764 (2006) 371.
- [31] V. Serfling et al., Phys. Rev. Lett. 80 (1998) 3928.
- [32] W. Trautmann in: W. Bauer, H. G. Ritter (Eds), Advances in Nuclear Dynamics, vol. 4, Plenum Press, New York, 1998 p. 349.
- [33] A. H. Raduta, Ad. R. Raduta, Nucl. Phys. A 703 (2002) 876.
- [34] S. Wuenschel et al., Nucl. Phys. A 843 (2010) 1.
- [35] H. Zheng, A. Bonasera, Phys. Lett. B 696 (2011) 178.

- [36] H. Zheng, A. Bonasera, Phys. Rev. C 86 (2012) 027602.
- [37] J. Rizzo et al., Phys. Rev. C 76 (2007) 024611.
- [38] G. Tăbăcaru et al., Eur. Phys. J. A 18 (2003) 103.
- [39] S. Levit, P. Bonche, Nucl. Phys. A 437 (1985) 426.
- [40] N. Marie et al. (INDRA Collaboration), Phys. Rev. C 58 (1998) 256.
- [41] S. Hudan et al. (INDRA Collaboration), Phys. Rev. C 67 (2003) 064613.
- [42] C. Hartnak et al., Eur. Phys. J. A 1 (1998) 151.
- [43] A. Ono, Phys. Rev. C 59 (1999) 853.
- [44] A. Le Fèvre et al., Phys. Rev. C 80 (2009) 044615.
- [45] B. Borderie et al. (INDRA Collaboration), Phys. Rev. Lett. 86 (2001) 3252.